EUROPEAN ORGANIZATION FOR NUCLEAR RESEARCH

CERN-EP/88-55
May 4th, 1988

CHARGE STRUCTURE OF THE HADRONIC FINAL STATE IN DEEP-INELASTIC MUON-NUCLEON SCATTERING

The European Muon Collaboration

Aachen[1], CERN[2], DESY (Hamburg)[3], Freiburg[4], Hamburg (University)[5], Kiel[6], LAL (Orsay)[7], Lancaster[8], LAPP (Annecy)[9], Liverpool[10], Marseille[11], Mons[12], MPI (München)[13], Oxford[14], RAL (Chilton)[15], Sheffield[16], Torino[17], Uppsala[18], Warsaw[19], Wuppertal[20]

M.Arneodo[17], A.Arvidson[18], J.J.Aubert[11], B.Badełek[19A], J.Beaufays[2], C.P.Bee[8B], C.Benchouk[11], G.Berghoff[1], I.Bird[8C], D.Blum[7], E.Böhm[6], X.de Bouard[9], F.W.Brasse[3], H.Braun[20], C.Broll[9†], S.Brown[10D], H.Brück[20E], H.Calen[18], J.S.Chima[15F], J.Ciborowski[19A], R.Clifft[15], G.Coignet[9], F.Combley[16], J.Coughlan[8G], G.D'Agostini[11], S.Dahlgren[18], F.Dengler[13], I.Derado[13], T.Dreyer[4], J.Drees[20], M.Düren[1], V.Eckardt[13], A.Edwards[20H], M.Edwards[15], T.Ernst[4], G.Eszes[9I], J.Favier[9], M.I.Ferrero[17], J.Figiel[5J], W.Flauger[3], J.Foster[16K], J.Ftáčnik[13], E.Gabathuler[10], J.Gajewski[5], R.Gamet[10], J.Gayler[3], N.Geddes[14G], P.Grafström[18], F.Grard[12], J.Haas[4], E.Hagberg[18], F.J.Hasert[1L], P.Hayman[10], P.Heusse[7], M.Jaffré[7], A.Jacholkowska[2], F.Janata[5], G.Jancsó[13I], A.S.Johnson[14M], E.M.Kabuss[4], G.Kellner[2], V.Korbel[3], J.Krüger[20E], S.Kullander[18], U.Landgraf[4], D.Lanske[1], J.Loken[14], K.Long[14N], M.Maire[9], P.Malecki[13J], A.Manz[13], S.Maselli[13], W.Mohr[4], F.Montanet[11], H.E.Montgomery[2O], E.Nagy[9I], J.Nassalski[19P], P.R.Norton[15], F.G.Oakham[15Q], A.M.Osborne[2], C.Pascaud[7], B.Pawlik[13J], P.Payre[11], C.Peroni[17], H.Peschel[20], H.Pessard[9], J.Pettinghale[10], B.Pietrzyk[11], U.Pietrzyk[20], B.Pönsgen[5], M.Pötsch[20], P.Renton[14], P.Ribarics[13I], K.Rith[4C], E.Rondio[19C], A.Sandacz[19P], M.Scheer[1], A.Schlagböhmer[4], H.Schiemann[5], N.Schmitz[13], M.Schneegans[9], A.Schneider[20], M.Scholz[1], T.Schröder[4], K.Schultze[1], T.Sloan[8], H.E.Stier[4], M.Studt[5], G.N.Taylor[14], J.M.Thénard[9], J.C.Thompson[15], A.de la Torre[5R], J.Toth[9I], L.Urban[1], L.Urban[9I], W.Wallucks[4], M.Whalley[16S], S.Wheeler[16], W.S.C.Williams[14], S.J.Wimpenny[10N], R.Windmolders[12] and G.Wolf[13]

(Submitted to Zeitschrift für Physik C)

1. *III Physikalisches Institut A, Physikzentrum, RWTH, D-5100 Aachen, Fed. Rep. Germany*
2. *CERN, CH-1211 Geneva 23, Switzerland*
3. *DESY, Notkestr. 85, D-2000 Hamburg 52, Fed. Rep. Germany*
4. *Fakultät für Physik, Universität Freiburg, Hermann – Herder Strasse 3, D-7800 Freiburg, Fed.Rep. Germany*
5. *II Institut für Experimentalphysik, Universität Hamburg, Luruper Chaussee 149, D-2000 Hamburg 50, Fed. Rep. Germany*
6. *Institut für Kernphysik, Universität Kiel, Olshausenstr. 40–60, D-2300 Kiel, Fed. Rep. Germany*
7. *Laboratoire de l'Accélérateur Linéare (LAL), Université de Paris-Sud, Bâtiment 200, F-91405 Orsay Cedex, France*
8. *Department of Physics, University of Lancaster, Bailrigg, Lancaster LA1 4YB, UK*
9. *Laboratoire d'Annecy-le-Vieux de Physique des Particules, B.P. 909, F-74019 Annecy-le-Vieux Cedex, France*
10. *Oliver Lodge Laboratory, Department of Physics, University of Liverpool, Oxford St., P.O. Box 147, Liverpool L69 3BX, UK*
11. *Centre de Physique de Particules, Faculté de Sciences de Luminy, Case 907, 70, route Léon Lachamp, F-13288 Marseille Cedex 9, France*
12. *Faculté des Sciences, Université de l'Etat à Mons, Avenue Maistriau 19, B-7000 Mons, Belgium*
13. *Max Planck Institut für Physik und Astrophysik, Föhringer Ring 6, Postfach 401212, D-8000 München 40, Fed. Rep. Germany*
14. *Nuclear Physics Laboratory, University of Oxford, Keble Road, Oxford OX1 3RH, UK*
15. *Rutherford and Appleton Laboratory, Chilton, Didcot OX11 0QX, UK*
16. *Department of Physics, University of Sheffield, The Hick's Building, Sheffield S3 7RH, UK*
17. *Instituto di Fisica, Università di Torino, Corso M. d'Azeglio 46, I-10125 Torino, Italy*
18. *Gustav Werners Institut, University of Uppsala, P.O. Box 531, S-75121 Uppsala, Sweden*
19. *Institute of Experimental Physics, University of Warsaw and Institute for Nuclear Studies, Hoża 69, PL-00-681 Warsaw, Poland*
20. *Fachbereich Physik, Universität Wuppertal, Gauss Strasse 20, Postfach 100 127, D-5600 Wuppertal, Fed. Rep. Germany*

A. *University of Warsaw, Poland.*
B. *Now at University of Liverpool, UK.*
C. *Now at MPI für Kernphysik, Heidelberg, Fed. Rep. Germany.*
D. *Now at TESA S.A., Renens, Switzerland.*
E. *Now at DESY, Hamburg, Fed. Rep. Germany.*
F. *Now at British Telecom, Ipswich, England.*
G. *Now at RAL, Chilton, Didcot, UK.*
H. *Now at Jet, Joint Undertaking, Abington, UK.*
I. *Permanent address: Central Research Institute for Physics of the Hungarian Academy of Science, Budapest, Hungary.*
J. *Permanent address: Institute of Nuclear Physics, Kraków, Poland.*
K. *Now at University of Manchester, England.*
L. *Now at Krupp Atlas Elektronic GmbH, Bremen, Fed. Rep. Germany.*
M. *Now at SLAC, Stanford, California, U.S.A.*
N. *Now at CERN, Geneva, Switzerland.*
O. *Now at FNAL, Batavia, Illinois, U.S.A.*
P. *Institute for Nuclear Studies, Warsaw, Poland.*
Q. *Now at NRC, Ottawa, Canada.*
R. *Now at Universidad Nacional, Mar del Plata, Argentina.*
S. *Now at University of Durham, UK.*
†. *Deceased*

ABSTRACT

The general charge properties of the hadronic final state produced in $\mu^+ p$ and $\mu^+ d$ interactions at 280 GeV are investigated. Quark charge retention and local charge compensation is observed. The ratio F_2^n/F_2^p of the neutron to proton structure function is derived from the measurement of the average hadronic charge in μd interactions.

1. Introduction

The leptoproduction of hadrons is generally interpreted in terms of the Quark-Parton Model (QPM). In this scheme the deep-inelastic muon-nucleon interaction is described by the scattering of the virtual photon, emitted by the muon, off a constituent quark (or antiquark). The excited parton system (quark-diquark in the simplest case) then fragments into the direct hadrons, some of them being resonances which subsequently decay into the final hadrons. Thus the general charge properties of the hadronic final state are determined by the charges of the primary partons and the nature of the fragmentation process. In addition they are influenced by the resonance decays. These considerations are illustrated in Fig.1 which shows the quark diagram corresponding to a typical μp interaction. In this figure the hadronisation process has been represented by the simplest chain of quark-antiquark pairs which has however all the qualitative properties of more refined models. This mechanism leads to the general properties of quark charge retention and local charge compensation.

In this paper we present results on the charge structure of the hadronic final state produced in deep-inelastic μp and μd interactions at 280 GeV. This experiment offers a unique opportunity to study the hadronisation because of the relative simplicity of the primary parton system, the full knowledge of the event kinematics (especially the virtual photon direction), nearly complete detection of the final state hadrons, and extended particle identification. The following aspects of the data are studied: the rapidity distribution of the hadronic net charge, the average charge of hadrons produced in given phase space regions, the long-range charge correlations and the probability distribution of the charge transfer. By comparing the charge properties of hadrons produced on hydrogen and deuterium targets some information on the

neutron structure is deduced.

This work continues the line of our previous publications on charge retention [1] and charge correlations [2].

2. Experimental procedure

The data presented come from the NA9 experiment performed at CERN at the 280 GeV M2 μ^+ beam, using the EMC spectrometer [3]. The apparatus detected tracks with momenta down to 200 MeV/c and gave essentially 4π coverage in the hadronic centre of mass (c.m.) system.

In order to restrict the event sample to regions where the corrections for event acceptance, smearing effects and radiative corrections are relatively small ($\lesssim 10\%$) the following selection criteria were applied:

$$4GeV^2 < Q^2, \qquad 20GeV < \nu < 260GeV, \qquad 4GeV < W < 20GeV,$$

$$E_{\mu'} > 20GeV, \qquad \frac{\nu}{E_\mu} < 0.9, \qquad \Theta_{\mu'} > 0.75^o$$

In this list Q^2 is the square of the four–momentum transfer between the incident muon and the target proton, E_μ and $E_{\mu'}$ are the energy of the incident and the scattered muon, respectively, in the laboratory system, $\nu = E_\mu - E_{\mu'}$ is the corresponding energy transfer, W is the total energy of the final state hadrons in their c.m. system, and $\Theta_{\mu'}$ is the laboratory angle between the incident and scattered muon. The number of events remaining after these cuts was about 25000 for μp and 20000 for μd scattering.

About 50% of all charged hadrons were identified using the Cherenkov and time of flight counters [4]. A special procedure described in [1] was applied to find additional slow protons. A Monte-Carlo simulation showed that it gave the correct mass assignment in 80% of the cases.

The data presented were corrected for the effects of acceptance, identification inefficiency, smearing introduced by the resolution of the apparatus, and inefficiencies of various off-line processors. The corrections were determined by a complete Monte-Carlo (MC) simulation of the experiment. Deep-inelastic scattering events

were generated using the Lund string model for the fragmentation process [5]. Radiative effects due to QED processes and secondary interactions of produced hadrons in the target were taken into account. The secondary particles were tracked through the apparatus and the multiple Coulomb scattering and effects of chamber inefficiencies were included. The resulting computed coordinates of the simulated measurements in each detector component were passed through the reconstruction program chain. Then, for a given data distribution, the correction function was computed as the ratio of the corresponding distributions for generated MC events and MC events after the experimental simulation. The corrected experimental distribution was then obtained by multiplying the measured distribution by the corresponding correction function. Unless stated to the contrary all the errors discussed below are statistical only.

3. The distribution of hadronic net charge

The distribution of the hadronic net charge as a function of the c.m. rapidity y is defined as the difference of the normalised rapidity distributions for positive and negative hadrons:

$$\frac{dQ}{dy} = \frac{1}{N_{ev}}\left(\frac{dN^+}{dy} - \frac{dN^-}{dy}\right) \tag{1}$$

where N_{ev} is the number of selected events. In our previous publication [1] it was pointed out that this distribution shows a structure which reflects the charges of the interacting partons. Since that time the event sample in the experiment has been more than doubled, allowing the analysis to be repeated in a more restricted region of hadronic energy, namely $10 < W < 20\ GeV$. This restriction to higher energy yields a broader rapidity range in which the current and target fragments are better separated. In Figs.2a-c the net charge distribution is shown in three intervals of Bjorken x for μp scattering. The errors indicated are statistical only. The systematic errors, reflecting the uncertainty of the MC correction, are estimated to be of similar magnitude.

A systematic change of the shape of the net charge distribution with increasing x is observed: at low x most of the positive charge is produced in the backward c.m. hemisphere. With increasing x the net charge in the forward hemisphere increases. This increase occurs mainly at higher values of rapidity ($y > 1.0$) and hence is not

simply due to spillover of target fragments. The observed x-dependence is easily explained in the QPM since at higher x scattering off a valence u-quark becomes dominant. For $x > 0.2$ the excess of positive charge is concentrated in two separated regions corresponding to fast backward and fast forward hadrons. This phenomenon is known as quark charge retention. The two maxima in the net charge distribution corresponding to quark and diquark fragments are separated by a central, essentially neutral region. Hadrons produced in this region compensate their charges locally and do not "remember" the charges of the primary partons. It is worth noting that the Lund string model, which incorporates these ideas, reproduces the data reasonably well.

In this context it is interesting to analyse the net charge distribution of hadrons produced in μd interactions (excluding the spectator protons which in general stop in the target and remain undetected). In this case the charge of the final hadrons is determined also by the relative probabilities of muon scattering on a neutron and a proton. In the impulse approximation these probabilities are given by the ratio of the structure functions F_2^n and F_2^p which of course depend on x.

In Figs.2d-f the distribution of the hadronic net charge in μd scattering is shown as a function of the c.m. rapidity in the same three x bins for the hadronic energy range $10 < W < 20\ GeV$. Clear differences are visible between the μp and μd distributions. The difference between their integrals (average total charge) is of course due to the contribution from μn scattering with total hadronic charge zero. In the backward hemisphere the net charge in μp interactions is always greater than that in μd scattering and the difference does not vary strongly with x. In the forward hemisphere, on the other hand, the net charge at low x is similar in both reactions and close to zero. This is easy to understand since in this x region scattering both on a proton and a neutron is dominated by sea quarks and antiquarks. At higher x values the net forward charge in μp interactions becomes systematically bigger than in μd interactions, due to the growing importance of the scattering off u-quarks in the proton. This aspect will be studied quantitatively in the next section.

4. The x-dependence of integrated charges

As noted before, the average total hadronic charge in μd interaction $< Q >^d$ is

related to the ratio of the neutron and proton structure functions. Neglecting the nuclear effects coming from the Fermi motion in the deuteron, which are $< 2\%$ for $x < 0.7$ [6], this relationship is given by:

$$\frac{F_2^n(x)}{F_2^p(x)} = \frac{1}{< Q(x) >^d} - 1 \qquad (2)$$

The average total charge $< Q(x) >^d$ (excluding the proton spectator, which is not detected) can be calculated as the difference of the MC-corrected average multiplicities of positive and negative hadrons in a given x interval. Thus eq.(2) offers a possibility of measuring the ratio of the neutron and proton structure functions F_2 using only the deuterium target. In Fig.3a the average hadronic charge in μd interactions is shown as a function of x. It starts from about 0.5 at low x and rises slowly with increasing x. This trend is reasonably well reproduced by the theoretical prediction based on the structure function parametrisation of Glück, Hoffmann and Reya [7] (see curve). The corresponding ratio of the neutron to proton structure functions, calculated using eq.(2), is shown in Fig.3b. The quoted errors are statistical only, the systematic errors are estimated to vary from $+0.1/-0.2$ at $x = 0$ to ± 0.1 at $x = 0.6$. For comparison we also present in Fig.3b the results from the standard determination of structure functions in deep-inelastic muoproduction [6] and electroproduction [8]. Although the accuracy of the present evaluation cannot compete with that of dedicated measurements, the results on the F_2^n/F_2^p ratio obtained in different ways look rather consistent: at x close to zero both structure functions are practically equal, but with increasing x the neutron to proton ratio falls below 0.5. In other words, at higher x deep-inelastic μd scattering is dominated by the proton interaction. This is a consequence of the quark content of the neutron and proton and the proportionality of the virtual-photon quark coupling to the square of the quark charge. Thus this constitutes a test of one of the basic assumptions in the quark parton model.

The average charge $< Q_F >$ of hadrons produced in the forward hemisphere of the c.m. system is the other integrated quantity of particular interest. It has been pointed out [1] that its value is essentially determined by the charge of the fragmenting quark and the analysis of sect.3 supports this view. Thus, a different x-dependence of $< Q_F >$ in μp and μd interactions is expected. The results are shown in Fig.4: at low x the average forward charges in interactions on protons and

deuterons are the same, whereas with increasing x the former grows faster than the latter. This behaviour reflects the relative contributions of neutron and proton and their different quark contents.

In order to test the idea of quark charge retention in a quantitative way we compare the measured forward charge in Fig.4 with the predictions of the QPM, in which the mean net charge of hadrons in the quark fragmentation region is given by [9]:

$$< Q_F >= \sum_i (e_i - \eta_i)\epsilon_i(x) \tag{3}$$

with

$$\epsilon_i(x) = e_i^2 q_i(x) / \sum_j e_j^2 q_j(x) \tag{4}$$

where the summation is over the quarks and antiquarks. Here e_i and $q_i(x)$ are the charge and the density distribution of a quark or antiquark with flavour i. The quantity $\eta_i = \eta$ or $-\eta$ for quarks or antiquarks respectively, where η is the "charge leakage", i.e. the charge of a "mean" quark produced in the fragmentation chain (Fig.1). The value has been estimated to be about 0.1 [1]. Using equations (3) and (4), together with the quark density distributions $q_i(x)$ of [7], $< Q_F >$ has been evaluated and the results are shown in Fig.4 as continuous lines. The agreement between data and the prediction of the QPM is good.

In the present experiment it has not been possible to select from the μd interactions the subsample of μn interactions event by event. However, from knowledge of the average forward charges in μp and μd interactions ($< Q_F >^p$ and $< Q_F >^d$ respectively) and the average total charge in μd interactions, $< Q >^d$, the average forward charge in μn interactions can be calculated, giving

$$< Q_F >^n = (< Q_F >^d - < Q >^d < Q_F >^p)/(1 - < Q >^d) \tag{5}$$

This is shown as a function of x in Fig.4. The resulting value is significantly different from zero, which demonstrates the presence of the charged constituents of the neutron.

5. Long-range charge correlations

Recently W.Ochs [10] has suggested a new kind of long-range charge correlation. His proposal concerns the average charges and the associated charge correlation in reduced regions c of the forward and backward hemispheres:

$$< Q_{F,B} >^c = \frac{1}{N_{ev}} \sum_{\alpha} Q^{\alpha}_{F,B} \quad \text{and} \quad < Q_F Q_B >^c = \frac{1}{N_{ev}} \sum_{\alpha\beta} Q^{\alpha}_{F} Q^{\beta}_{B} \tag{6}$$

Here $Q^{\alpha}_{F,B}$ is the charge of an individual hadron α in region c and the summation is over all such hadrons in the N_{ev} events. The "full" forward charge $< Q_F >$ studied in sect.4 is for the special case in which the selected region c is the whole forward hemisphere. We also define the normalised charge correlation function:

$$R_Q = \frac{< Q_F Q_B >^c}{< Q_F >^c < Q_B >^c} \tag{7}$$

In the framework of the QPM the theoretical expectation for R_Q can be readily calculated using two simple assumptions. In the simplest version of this model, the fragmenting quark (antiquark) of charge e_i picks up an antiquark (quark) of arbitrary flavour to form a meson with an average charge of $Q_i = e_i - \eta_i$ (η_i has been defined in sect.4.), normally accompanied by other hadrons of total charge zero. This charge Q_i is distributed over the forward hemisphere. It should be noted that the complications introduced by the creation of baryons and antibaryons are neglected in this approach. We assume that the hadron charge in the selected forward region c is proportional to Q_i with a flavour independent factor f^c_F, so that

$$< Q_F >^c = \sum_i f^c_F (e_i - \eta_i) \epsilon_i \tag{8a}$$

Correspondingly for the backward hemisphere:

$$< Q_B >^c = \sum_i f^c_B (1 - e_i + \eta_i) \epsilon_i \tag{8b}$$

Equation (8b) is for μp scattering where the total hadronic charge is one. (For the full forward or backward hemisphere f^c_F or f^c_B is unity.)

The second assumption is that for the forward-backward charge correlation the following factorisation property holds:

$$< Q_F Q_B >^c = \sum_i f^c_F (e_i - \eta_i) f^c_B (1 - e_i + \eta_i) \epsilon_i \tag{9}$$

If only one quark flavour is involved (e.g. in νp scattering at large x) the factorisation in eq.(9) means that the charge distributions in the two hemispheres are uncorrelated and $R_Q = 1$. In the more general case of a superposition of processes involving several quark flavours the same assumption leads to a long-range correlation, i.e. $R_Q \neq 1$. For example in μp scattering at high x where the contribution from the sea quarks is negligible and assuming $u \approx 2d$ one obtains $R_Q \approx 0.6$.

The correlation function R_Q is plotted in Fig.5 for μp events with $x > 0.2$ as a function of an increasing "cut-off" parameter x_F^c (x_F is the Feynman variable). The consecutive data points correspond to a more and more restrictive selection of the fragmentation region: for a given value of x_F^c only particles with $|x_F| > x_F^c$ are included, i.e. particles inside a symmetric "window" of $-x_F^c < x_F < x_f^c$ are rejected. The prediction according to eqs.(8) and (9) is plotted as a horizontal dashed line. (The f-factors cancel in the ratio R_Q). The measured values at low x_F^c are seen to be far from this prediction. However after a rapid rise R_Q becomes approximately constant for $x_F^c \gtrsim 0.3$ and the data points are reasonably close to the expectation. This means that the charges of hadrons in the two opposite "extreme" fragmentation regions are consistent with showing only correlations predicted by the QPM in eq.(9). Thus, the observed long-range charge correlation ($R_Q \neq 1$) can be entirely explained by the superposition of processes with various (anti)quark flavours, each with uncorrelated charges in the two hemispheres. The negative values of R_Q observed for x_F^c around zero is a consequence of charge conservation with total charge 1 and of $< Q_F >$ and $< Q_B >$ being positive. This can easily be seen by considering the possible charges Q_F and Q_B, constrained by $Q_F + Q_B = 1$. The full curve in Fig.5 is the prediction of the Lund-model; it agrees well with the data.

It has been pointed out [10] that R_Q is very sensitive to the form of the hadronisation mechanism. For example, in the Firestring Model (FSM) [11] the final state hadrons are produced via the decay of "firestrings" with integer charge. In this model the phase of the primary parton evolution is absent (in contrast to the QPM-QCD models) and the final state is the result of a "hadron phase" evolution only (another one-phase model is discussed in [12] for e^+e^- annihilation). Many aspects of the present μp experiment have been compared to the predictions of the FSM [13, 14] and it is found to give a reasonably good qualitative description of the data. Using a sample of MC generated events, the prediction of the FSM for R_Q is

plotted as a dashed-dotted line in Fig.5 and is seen to be in complete disagreement with the experiment.

In Fig.6 R_Q (for $x_F^c = 0.5$) is plotted as a function of x for μp events (full points) together with the prediction of the Lund model (open points). The full line represents the QPM expectation from eqs.(8) and (9). At lower x values where processes involving several (anti)quark flavours are superimposed, the agreement between the data and the QPM calculation is somewhat worse than for higher x, where only the two valence quarks u and d dominate. The expectation from a hadron-phase model (following [10]) is plotted as a dashed line. This calculation is performed assuming factorisation as in eqs.(8) and (9), but the primary quark states are replaced by a proper superposition of states with integer charges. The prediction of the FSM are found to be similar. This model deviates significantly both from the data and from the QPM.

6. The charge transfer distribution

The charge transfer ΔQ between the c.m. backward and forward hemispheres is a useful variable describing the charge properties of the hadronic final state. It is defined as the difference between the final and initial charges in the forward hemisphere, or equivalently, as the difference between the initial and final charges in the backward hemisphere. According to this definition, charge is transferred during the interaction from the backward to the forward hemisphere. So far most data on charge transfer come from hadron-hadron interactions [15]. In μp scattering the initial state has charge 1 in the backward (proton) and charge 0 in the forward hemisphere (virtual photon). Thus, the charge transfer ΔQ in a μp event is simply equal to the net charge Q_F of hadrons produced in the forward hemisphere:

$$\Delta Q = Q_F = 1 - Q_B \tag{10}$$

where Q_B denotes the net charge of hadrons produced in the backward hemisphere. In the QPM the charge transfer has a simple interpretation. On the level of the direct hadrons the charge of each cut quark line (of the interacting quark or from the fragmentation chain) contributes to the value of ΔQ. However the subsequent decays of resonances can considerably modify the initial value. These considerations are illustrated in Fig.1.

The probability distribution $P(\Delta Q)$ of the charge transfer is quite sensitive experimentally to any losses or pick-ups of charged tracks. Therefore a careful correction of the raw data is necessary. To do this, ΔQ was expressed by the directly measured numbers of positive and negative tracks in the forward hemisphere, n^+ and n^-:

$$\Delta Q = n^+ - n^- \tag{11}$$

The charge transfer distribution $P(\Delta Q)$ is related to the two-dimensional distribution $P(n^+, n^-)$ by the formula:

$$P(\Delta Q) = \sum_{\Delta Q = n^+ - n^-} P(n^+, n^-) \tag{12}$$

The latter distribution was corrected for experimental imperfections as described in sect.2. It follows from eq.(10) that the charge transfer distribution can be calculated independently using either the forward or the backward tracks. A comparison proved both results to be consistent and allowed the systematic errors on the ΔQ distribution to be estimated. These turned out to be comparable with the statistical errors.

The first two moments of the charge transfer distribution, namely its average value $< \Delta Q >$ and the dispersion squared $D^2 =< \Delta Q^2 > - < \Delta Q >^2$, are suitable for a quantitative study.

Fig.7 presents the probability distribution $P(\Delta Q)$ of the charge transfer in μp interactions in the whole energy range $4 < W < 20\ GeV$ together with the Lund model prediction (full line). The model generally agrees with the data except for the tails of the distribution. This discrepancy may be partly due to systematic uncertainties which are more pronounced in these regions. The experimental values of the moments are: $< \Delta Q >= 0.30 \pm 0.01$, $D^2 = 1.25 \pm 0.05$. These values can be compared with the Lund model expectations: $< \Delta Q >= 0.28, D^2 = 1.06$. The most probable values expected from the strict ordering of charges in the simple fragmentation chain of Fig.1. are $\Delta Q = -1, 0, 1$. Higher values of the charge transfer are expected to have small, but non-zero, probabilities as a consequence of the stochastic mechanism of quark-antiquark production in the fragmentation process.

To examine the influence of the overall charge conservation and finite hadron multiplicity on the charge transfer distribution a so-called Random Charge Model (RCM) was constructed. In each event the charges of the final hadrons were randomised in such a way that the total charge and multiplicity of the event and the momenta of the particles were unchanged. Thus all dynamical properties depending on the charges of the particles, apart from global charge conservation, were removed. As can be seen from Fig.7 (dashed curve) the RCM charge transfer distribution is not in agreement with the data and also differs significantly from the Lund model prediction (full curve). The RCM distribution is broader than the data and its maximum is shifted towards $\Delta Q = 1$. The RCM values of the moments are $< \Delta Q >= 0.56$ and $D^2 = 1.55$. The fact that the experimental value of the dispersion is smaller than that of the RCM can be interpreted as a consequence of local charge compensation following from the quark ordering in the fragmentation chain of Fig.1. On the other hand, the difference between the experimental and the RCM average charge transfer again demonstrates the retention of the charge of the interacting quark.

7. The dependence of the charge transfer distribution on event variables

As discussed already in sect.4 the average forward charge (=average charge transfer) reflects mainly the charge of the interacting (anti)quark with a small contribution from the fragmentation chain. In case of the charge transfer dispersion squared D^2 the situation is rather different: the contribution from the fragmentation chain may dominate over that of the interacting quark. Therefore investigating the x and W dependence of D^2 may yield interesting information about the hadronisation process. Because of the stochastic character of this process one can also expect a dependence of D^2 on the charged multiplicity. The interpretation of the results is however obscured by the $x - W$ correlation following from the relation:

$$W^2 = M^2 + Q^2(\frac{1}{x} - 1), \tag{13}$$

where M denotes the target mass. According to this relation an x dependence may show up in a W-dependence, and vice-versa.

In order to reduce these mutual reflections the W-dependence of D^2 is plotted in Fig.8 for fixed x intervals. In a fixed W bin, D^2 does not seem to depend on

x, implying that it is essentially independent of the number of interacting quark flavours. In a given x interval the dispersion evidently increases with rising W and the source of this rise should be looked for in the hadronisation process. Following this line, D^2 is shown in Fig.9 as a function of the charged multiplicity, n_{ch}, together with the prediction from the RCM. Both the data and the RCM show a strong linear rise of D^2 with the multiplicity, typical of a chaotic process. However the data have a significantly lower slope. The observed behaviour of the data implies that the dispersion of the charge transfer distribution is determined by the short range ordering of particle charges which has a stochastic character. (Absolute ordering of direct hadrons in the fragmentation chain would yield a D^2 independent of multiplicity). In other words, a certain degree of chaos is a natural feature of the hadronisation process and this is reflected in the strong dependence of D^2 on the multiplicity. For example, the resonance decays effectively increase the value of the dispersion because they increase the charged multiplicity of the final state. In this context the W-dependence of D^2 observed in Fig.8 turns out to be a reflection of its genuine multiplicity dependence, the average multiplicity increasing with rising W like lnW [16]. This is illustrated more directly in Fig.10, where the W-dependence of D^2 for fixed charged multiplicities is presented. At fixed multiplicity the dispersion is constant or, for $n_{ch} > 5$, decreases with increasing W. The latter observation can be understood on the basis of kinematical arguments: at fixed multiplicity a higher energy means a larger average rapidity distance between particles, and thus more effective ordering of their charges. This, in consequence, leads to a smaller dispersion of the charge transfer.

In conclusion the width of the charge transfer distribution is found to be determined by the stochastic and local properties of the fragmentation process.

8. Summary

The general charge properties of the hadronic final state produced in deep-inelastic μN interactions at 280 GeV have been studied. They are found to be determined by the charges of the interacting partons and the mechanism of the fragmentation.

The retention of the quark charge by fast hadrons and local charge compensa-

tion in the central region are observed in the rapidity distributions of the hadronic net charge. The charge distribution in μd and μp interactions are clearly different reflecting the different flavours of the initial parton states in both targets.

The estimate of the neutron and proton structure function ratio F_2^n/F_2^p, derived from the total hadronic charge in μd interactions, is consistent with the results obtained by the standard measurement from proton and deuteron targets.

Significant long-range correlations have been observed between the charges in the forward and backward hemispheres. Within the QPM these correlations can be explained by the superposition of processes with various (anti)quark flavours, each with uncorrelated charges in the two hemispheres.

The charge transfer distribution and its moments have been measured. Its average value reflects mainly the charge of the interacting (anti)quark whereas its shape is determined mostly by the properties of the fragmentation process. In particular its dispersion depends strongly on the charged multiplicity.

The random distribution of particle charges is excluded by the data.

All aspects of the charge distributions which have been studied, are reasonably well reproduced by the Lund fragmentation model.

9. Acknowledgements

We would like to thank all people in the various laboratories who contributed to the construction, operation and analysis of this experiment. The support of the CERN staff in operating the SPS, muon beam and computer facilities is gratefully acknowledged. We are grateful to W.Ochs for valuable discussions and comments.

REFERENCES

[1] EMC, J.P.Albanese et al.,*Phys. Lett.* **144 B** (1984) 302.

[2] EMC, M.Arneodo et al.,*Z. Phys.* **C 31** (1986) 333.

[3] EMC, J.P.Albanese et al.,*Nucl. Instr. and Meth.* **212** (1983) 111.

[4] EMC, M.Arneodo et al.,*Phys. Lett.* **150 B** (1985) 458.

[5] B.Andersson et al.,*Phys. Rep.* **9 7** (1983) 31.

[6] EMC, J.J.Aubert et al.,*Nucl. Phys.* **B 293** (1987) 740.

[7] M.Glück, E.Hoffmann and E.Reya,*Z. Phys.* **C 13** (1982) 119.

[8] W.B.Atwood, SLAC-PUB-2428(1979),
A.Bodek et al.,*Phys. Rev.* **D 20** (1979) 1471.

[9] R.D.Field and R.P.Feynman,*Nucl. Phys.* **B 136** (1978) 1.

[10] W.Ochs,*Z. Phys.* **C 34** (1987) 397.

[11] G.Preparata, Proc. 11th SLAC Summer Institute on
Particle Physics 1983,p.395(1983)
L.Angelini et al., *Rivista N.Cimento* vol.6(1983),n.3

[12] W.Ochs,*Z. Phys.* **C 23** (1984) 131.

[13] EMC, M.Arneodo et al.,*Z. Phys.* **C 36** (1987) 527.

[14] E.Ferrari et al., Dipartimento di Fisica Universita di Roma "La Sapienza",
INFN, Sezione di Roma, Preprint N.578(1987).

[15] E.A.De Wolf,*Z. Phys.* **C 22** (1984) 87.
R.Göttgens et al.,*Nucl. Phys.* **B 193** (1981) 287.

[16] EMC, M.Arneodo et al.,*Nucl. Phys.* **B 258** (1985) 249.

FIGURE CAPTIONS

1. Quark diagram describing a typical μp interaction. The variable y denotes the c.m. rapidity, Q_F is the net charge of the hadrons produced in the forward hemisphere ($y > 0$).

2. Distribution of the hadronic net charge as a function of c.m. rapidity y in μp and μd interactions with $10 < W < 20$ GeV, in three x intervals: $x < 0.05$, $0.05 < x < 0.2$, $x > 0.2$.

3. a) Average total charge of hadrons (except the spectator) produced in μd interactions as a function of x. The line is obtained from eq.(2) using the structure function parametrisation of ref.[7] (see text). b) The x dependence of the ratio F_2^n/F_2^p of the neutron and proton structure functions. Open circles represent this experiment, full points are from the EMC-NA2 experiment [6] and the shaded area shows a compilation of the SLAC electroproduction data [8].

4. Average forward hadronic charge $< Q_F >$ as a function of x in μp (full points), μd (open circles), and μn (crosses) interactions. The curves represent the expectations from the QPM (see text).

5. The normalized charge correlation R_Q as a function of the cut-off x_F^c for events with $x > 0.2$. The full curve represents the Lund model, the dashed horizontal line is the expectation from the QPM and the dashed-dotted line is the prediction of the fire-string model.

6. The normalized charge correlation R_Q as a function of x. The full points are the data, the open circles are the Lund model prediction, both for a cut-off at $x_F^c = 0.5$ (see Fig.5). The continuous and dashed lines are the predictions of the QPM and a hadron-phase model [10] respectively.

7. The charge transfer distribution $P(\Delta Q)$ in μp interactions with $4 < W < 20$ GeV. The solid and dashed lines represent the predictions of the Lund model and of the Random Charge Model respectively.

8. The charge transfer dispersion squared D^2 as a function of W in three

x intervals: $x < 0.05$ (full circles), $0.05 < x < 0.20$ (full triangles) and $x > 0.2$ (full squares). The curves are the Lund model predictions.

9. The dispersion squared D^2 as a function of the charged hadron multiplicity n_{ch}. The full points represent the data, the open points are calculated from the RCM (data with randomised charge). The straight lines are linear fits to the points.

10. The dispersion D^2 as a function of W for fixed charged hadron multiplicities n_{ch}: $n_{ch} = 3$ (open triangles), $n_{ch} = 5$ (open circles), $n_{ch} = 7$ (full triangles), $n_{ch} = 9$ (full points). The curves are the Lund model predictions.

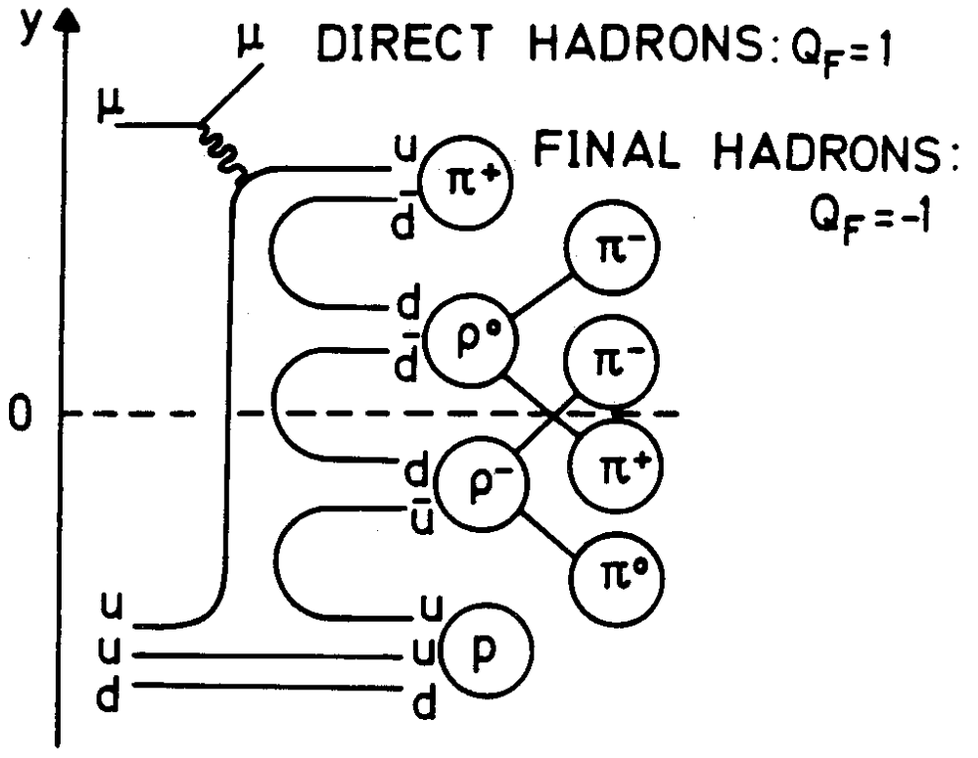
y
μ
μ
DIRECT HADRONS: $Q_F=1$
FINAL HADRONS:
$Q_F=-1$
u
d
π^+
d
$\bar{d}$
ρ^0
d
$\bar{u}$
ρ^-
u
u
d
u
u
d
p
π^-
π^-
π^+
π^0
0

Fig. 1

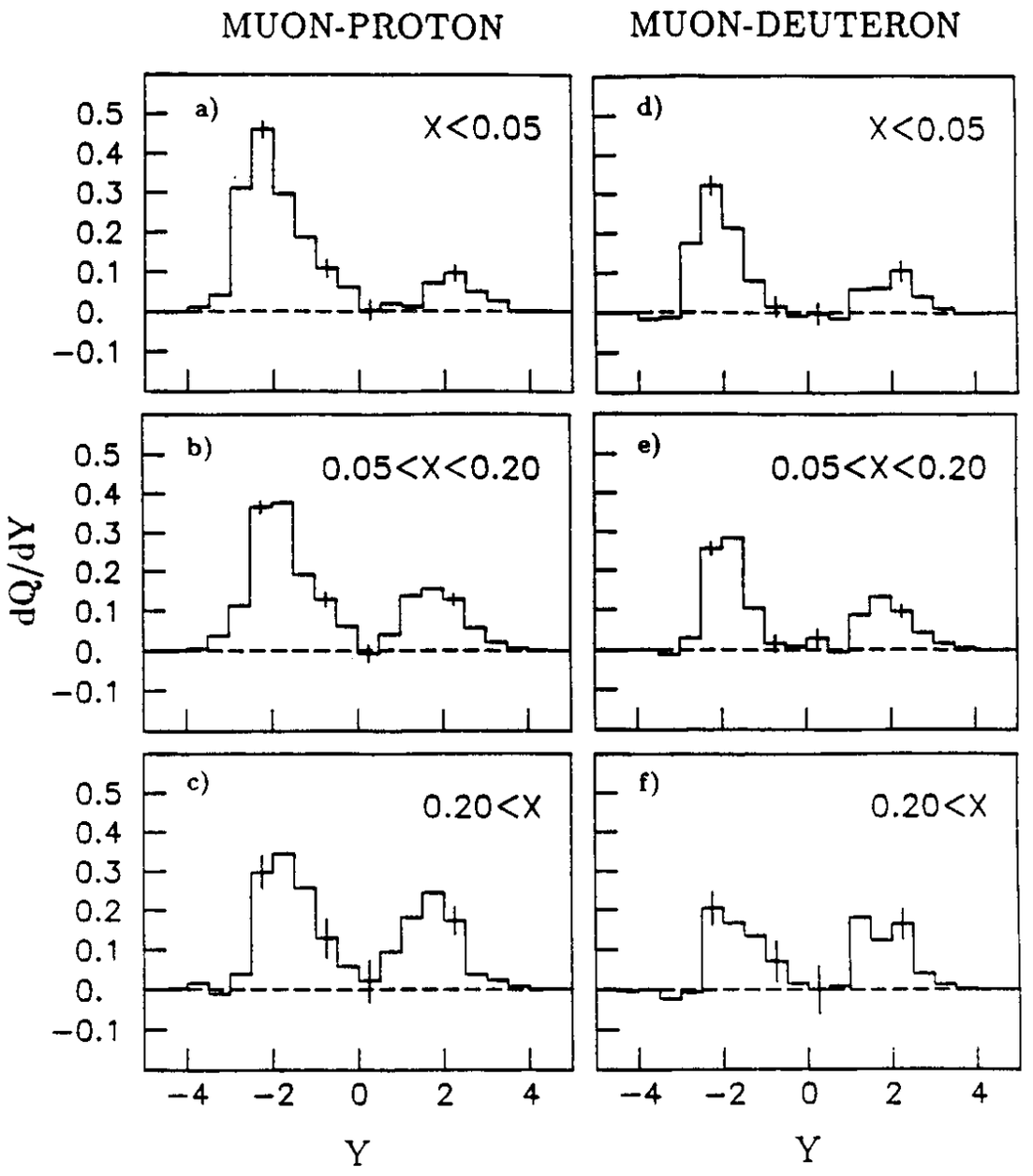
MUON-PROTON
MUON-DEUTERON
a)
X<0.05
d)
X<0.05
b)
0.05<X<0.20
e)
0.05<X<0.20
c)
0.20<X
f)
0.20<X
dQ/dY
0.5
0.4
0.3
0.2
0.1
0.
−0.1
−4
−2
0
2
4
Y

Fig. 2

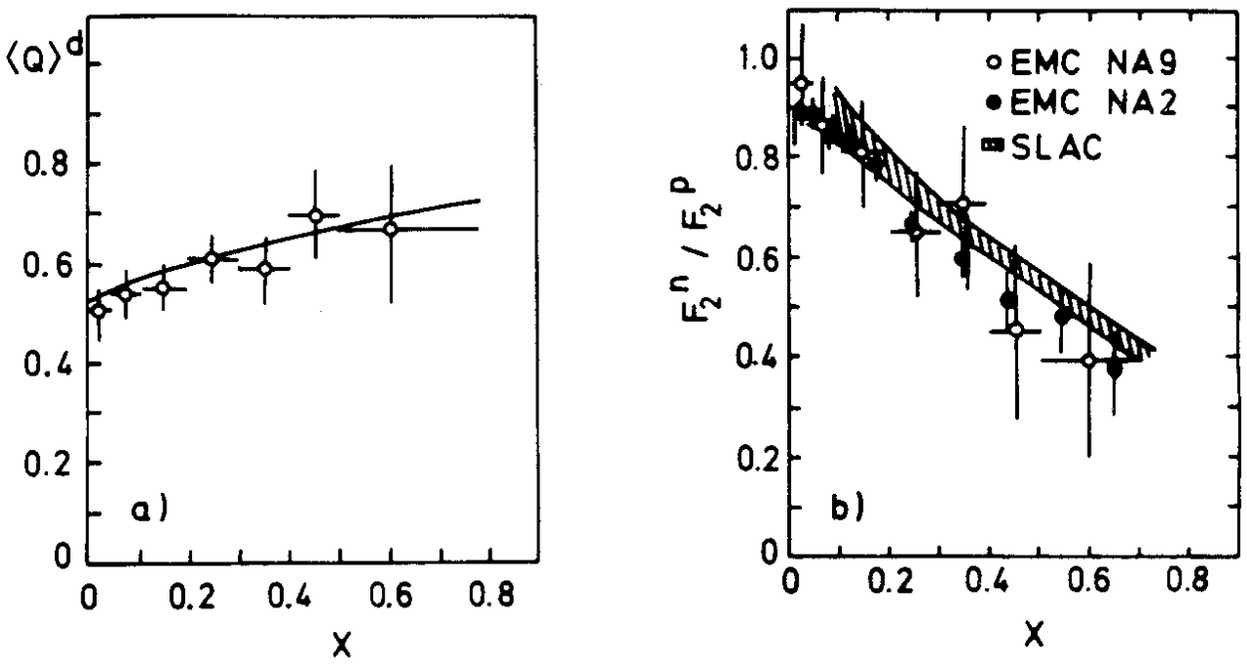
⟨Q⟩^d
0.8
0.6
0.4
0.2
0
a)
0
0.2
0.4
0.6
0.8
X
1.0
EMC NA9
EMC NA2
SLAC
F2^n / F2^p
b)
X

Fig. 3

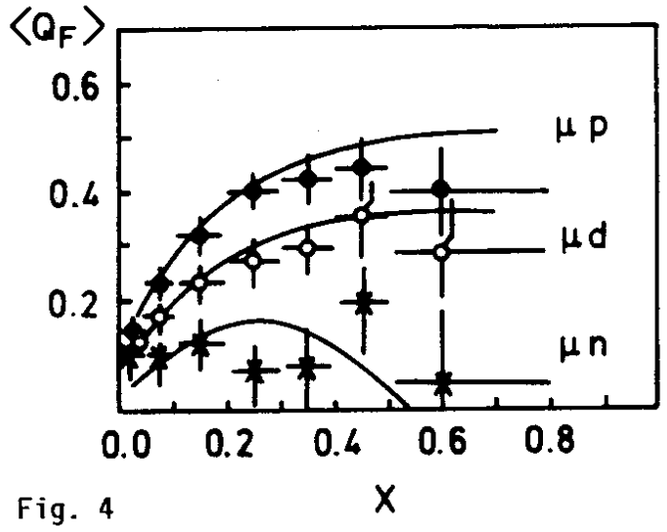
⟨Q_F⟩
0.6
0.4
0.2
μ p
μ d
μ n
0.0
0.2
0.4
0.6
0.8
X

Fig. 4

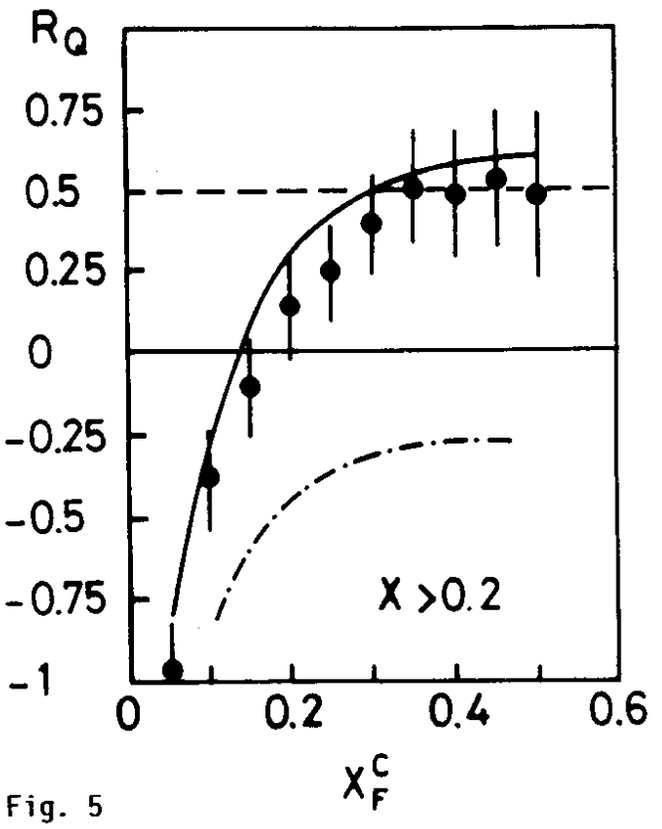

Fig. 5

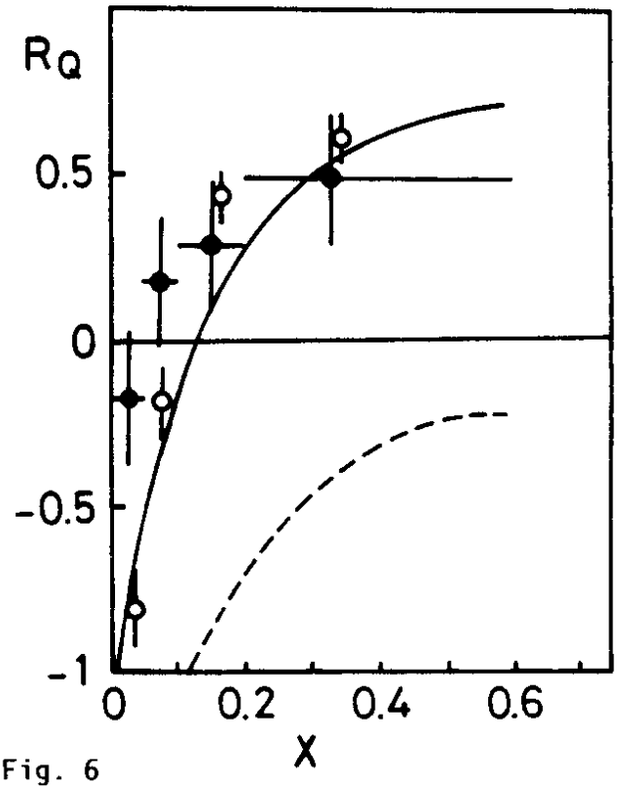

Fig. 6

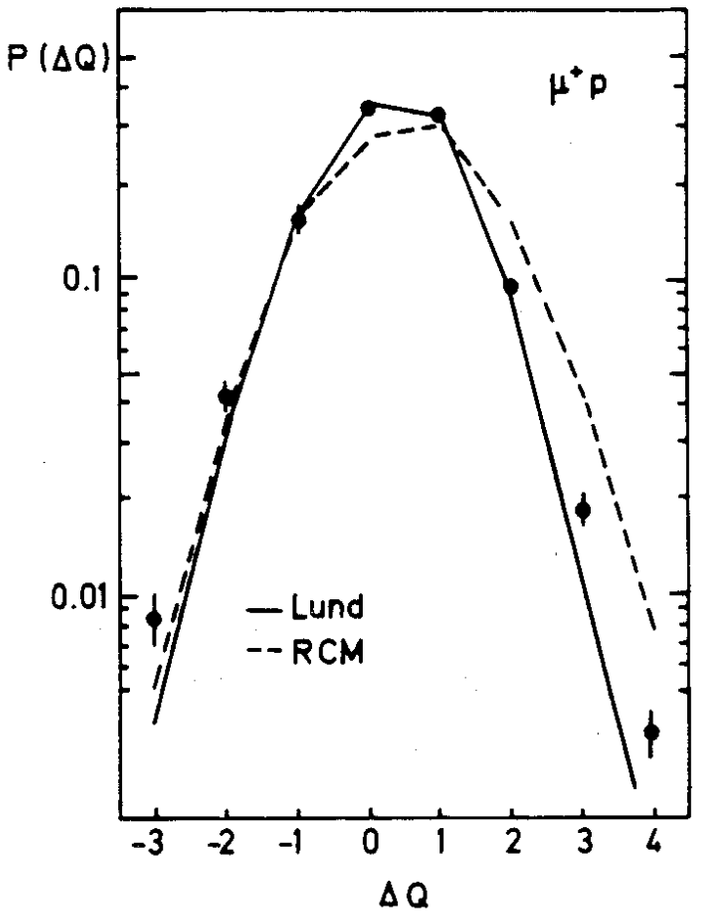
P (ΔQ)
μ⁺p
0.1
0.01
— Lund
-- RCM
-3
-2
-1
0
1
2
3
4
ΔQ

Fig. 7

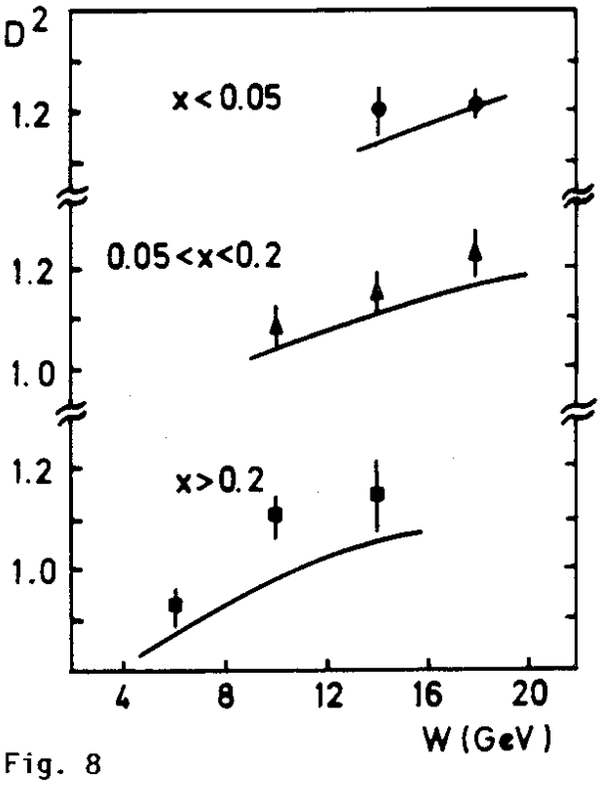
D²
x<0.05
1.2
0.05<x<0.2
1.2
1.0
x>0.2
1.2
1.0
4
8
12
16
20
W (GeV)

Fig. 8

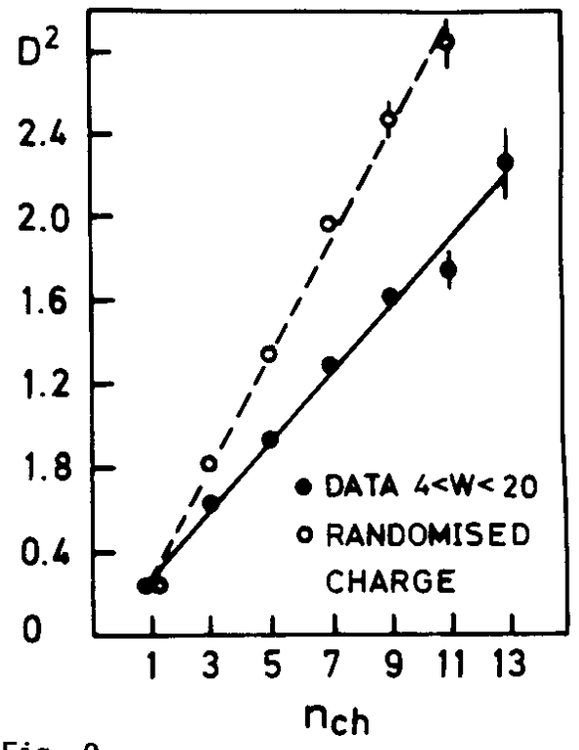
D²
2.4
2.0
1.6
1.2
1.8
0.4
0
1 3 5 7 9 11 13
nch
● DATA 4<W< 20
o RANDOMISED CHARGE

Fig. 9

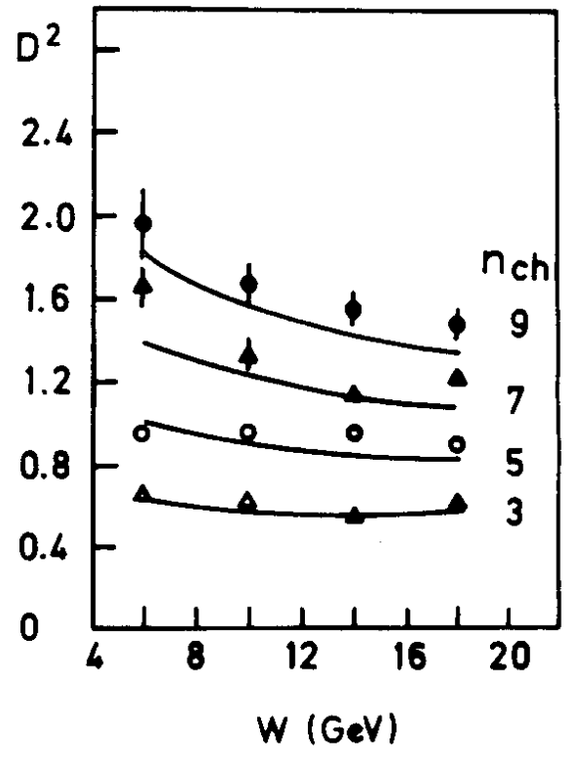
D²
2.4
2.0
1.6
1.2
0.8
0.4
0
4 8 12 16 20
W (GeV)
nch
9
7
5
3

Fig. 10